

# **B. TECH. PROJECT REPORT**

**On**

**“Investigation on Influence of Laser Anchoring  
of NiTi Shape Memory Alloy Towards  
Actuation Characteristics for Underwater Soft Robotics.”**

**by**

**YASH KASHIV**



**DEPARTMENT OF MECHANICAL ENGINEERING  
INDIAN INSTITUTE OF TECHNOLOGY  
INDORE  
&  
JABALPUR ENGINEERING COLLEGE  
JABALPUR  
MAY, 2024**

# **B. TECH. PROJECT REPORT**

**On**

**“Investigation on Influence of Laser Anchoring  
of NiTi Shape Memory Alloy Towards  
Actuation Characteristics for Underwater Soft Robotics.”**

**by**

**YASH KASHIV**



**DEPARTMENT OF MECHANICAL ENGINEERING  
INDIAN INSTITUTE OF TECHNOLOGY  
INDORE  
&  
JABALPUR ENGINEERING COLLAGE  
JABALPUR  
MAY, 2024**

**“Investigation on Influence of Laser Anchoring  
of NiTi Shape Memory Alloy Towards  
Actuation Characteristics for Underwater Soft Robotics.”**

**A PROJECT REPORT**

*Submitted in partial fulfillment of the requirements for the award of  
the degree of*

**BACHELOR OF TECHNOLOGY  
In  
MECHANICAL ENGINEERING**

*Submitted by:*

**Yash Kashiv**

*Guided by*

**Dr. I.A. Palani, Professor**

**Dr. Bhupendra Gupta, Associate Professor**

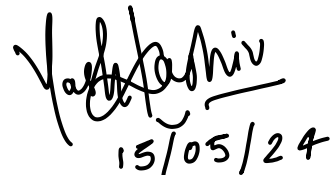


**DEPARTMENT OF MECHANICAL ENGINEERING  
INDIAN INSTITUTE OF TECHNOLOGY, INDORE  
&  
JABALPUR ENGINEERING COLLEGE, JABALPUR  
MAY, 2024**

## **CANDIDATE’S DECLARATION**

I hereby declare that the project entitled “**Investigation on Influence of Laser Anchoring of NiTi Shape Memory Alloy Towards Actuation Characteristics for Underwater Soft Robotics.**” submitted in partial fulfillment for the award of the degree of Bachelor of Technology in ‘Mechanical Engineering’ completed under the supervision of **Dr. I.A. Palani, Professor** IIT Indore and **Dr. Bhupendra Gupta, Associate Professor** JEC Jabalpur is an authentic work.

Further, I declare that I have not submitted this work for the award of any other degree elsewhere.



**Yash Kashiv**

**me2330203005/0203me201089**

**Signature of the student**

---

### **CERTIFICATE by BTP Guide(s)**

It is certified that the above statement made by the students is correct to the best of my/our knowledge.

---

**Dr. Bhupendra Gupta**

**Associate Professor**

**Signature of BTP Guide with date**

---

**Dr. I.A. Palani**

**Professor**

**Signature of BTP Guide with date**

## **Preface**

This report on “Investigation on Influence of Laser Anchoring of NiTi Shape Memory Alloy Towards Actuation Characteristics for Underwater Soft Robotics.” is prepared under the guidance of Prof. I.A. Palani and Prof. Bhupendra Gupta. Through this report, I have tried to develop a highly reliable SMA-PDMS actuator and increase its actuation characteristics.

I have tried to the best of my abilities and knowledge to explain the content in a lucid manner. I have included the figures and theory to explain the development and actuation.

**Yash Kashiv**

B. Tech IV Year

Discipline of Mechanical Engineering

IIT Indore

## **Acknowledgments**

I extend my heartfelt gratitude to **Prof. I.A. Palani** and **Prof. Bhupendra Gupta** for their invaluable support and expert guidance during my project and report preparation. Their regular and insightful discussions have been instrumental in providing me with valuable suggestions and ideas, greatly enhancing the quality of my thesis work.

I am deeply thankful to my seniors, **Dr. Nandini Patra, Dr. Anshu Sahu, Mr. Kaushal Gangwar, Mr. Arpit Kumar Singh, Ms. Diksha Jaurker, Mr. Vignesh R, Mr. Mohd. Washique Ahemad** and **Mr. Sayan Doloi** for their unwavering motivation and assistance throughout this project. I would like to express my sincere appreciation to **Mr. Ashwin Wagh** and **Mr. Krishnapal Tomar** for their generous cooperation and support.

I am thankful and indebted to my parents, grandparents, and my sister for their love and constant support.

**Yash Kashiv**

B. Tech IV Year

Discipline of Mechanical Engineering

IIT Indore

## **Abstract**

This report investigates the influence of laser anchoring on the actuation characteristics of NiTi shape memory alloy (SMA) for underwater soft robotics applications. Laser anchoring, a technique involving precise surface modifications via laser irradiation, was employed to enhance the adhesion between SMA wires and polydimethylsiloxane (PDMS). The study aimed to optimize the actuation performance of SMA-PDMS composite actuators by reducing slippage and improving energy efficiency.

We conducted experiments using NiTi wires with different laser power settings (12 W, 15 W, 17.5 W, and 20 W) and analyzed the surface characteristics and actuation performance of the laser-anchored samples compared to pristine wires. Results demonstrated that laser-anchored wires exhibited lower phase transformation temperatures, leading to reduced power requirements and enhanced actuation efficiency. Performance metrics such as angular displacement, angular velocity, and cycle frequency were evaluated across various voltage levels and frequencies.

The findings reveal that while pristine SMA wires initially outperformed laser-anchored wires at lower voltages, the latter showed superior performance at higher voltages and frequencies due to improved adhesion and reduced slippage. Additionally, the integration of laser-anchored SMA wires with PDMS resulted in better dynamic performance and reliability.

This study underscores the potential of laser anchoring as a technique to enhance the functionality of SMA actuators in underwater soft robotics, providing valuable insights for future developments in bio-inspired robotic systems.

# **TABLE OF CONTENT**

<b>Chapter 1: Introduction</b>	<b>10</b>
1.1 Bio-Inspired Soft Robotics	10
1.2 Shape Memory Alloy	11
1.3 Polydimethylsiloxane	12
1.4 3-D Printing of Mold Structure	13
1.5 Outline of the thesis	13
<b>Chapter 2: Literature Review</b>	<b>14</b>
<b>Chapter 3: Laser Anchoring and Laser Parameters</b>	<b>18</b>
3.1 Laser Anchoring	18
3.2 Laser Parameters	18
3.3 Laser Anchoring on 0.5 mm NiTi Wire	19
3.4 Actuation of Anchored and Pristine Wire	20
3.5 Laser Anchoring on 0.25 mm NiTi Wire	21
3.6 Summary	22
<b>Chapter 4: Fabrication of Laser-Anchored SMA-PDMS Structure</b>	<b>24</b>
4.1 Analytical Model	24
4.2 Fabrication Process	24
4.3 Double-Layer Clay Cover Modeling	26
4.4 Setup for electrical actuation	28
4.5 Summary	29
<b>Chapter 5: Results and Discussion</b>	<b>30</b>
5.1 Phase Transformation Analysis	30
5.2 Angular Displacement and Voltage	31
5.3 Angular Velocity and Voltage	32
5.4 Number of Cycles per Minute and Voltage	32
5.5 Angular Displacement at Different Frequencies and Voltage	33
5.6 Conclusion	34



## **TABLE OF FIGURE**

Figure 1: (a) A soft robotic gripper. (b) A soft manipulator modeled on the characteristic muscle structure of the octopus. (c) SMA wire embedded tongue. (d)Hydraulic based soft robotic jellyfish. ....	11
Figure 2: (a) Shape memory effect. (b) Super-elasticity.....	12
Figure 3: PDMS pouring and curing the composite into the oven .....	12
Figure 4: 3-D Printed Mold Structure.....	13
Figure 5:Turtle-based actuator using a composite structure .....	14
Figure 6:SMA wire/GFRP composite-based inchworm robots .....	15
Figure 7:BISMAC-based Robojelly .....	16
Figure 8:Dielectric elastomer-based jellyfish .....	16
Figure 9:(a) Laser anchoring using laser power 12 watt. (b) Laser anchoring using laser power 22 watt....	19
Figure 10:(a) &(d)Optical image with laser power 15 and 20 watts respectively. (b)&(e) Surface profilometry with laser power 15 and 20 watts respectively. (c)&(f)graph Height vs Horizontal distance. .	20
Figure 11:(a) &(d)Optical image with laser power 15 and 17.5 watts respectively. (b)&(e) surface profilometry with laser power 15 and 17.5 watts respectively. (c)&(f)graph Height vs Horizontal distance. ....	22
Figure 12:Analytical Model .....	23
Figure 13: Shape Deposition Manufacturing .....	23
Figure 14:Double-layer clay cover molding .....	23
Figure 15: Setup for Electrical Actuation .....	23
Figure 16:(a) Source code for actuation. (b)Top view of the SMA-PDMS Structure.....	23
Figure 17: Graph of Heat flow vs Temperature of Pristine and Laser Anchored NiTi Wire .....	23
Figure 18: Angular Displacement Vs Voltage .....	23
Figure 19: Angular Velocity Vs Voltage .....	23
Figure 20: No. of Cycles per Minute Vs Voltage.....	23
Figure 21: Angular Displacement vs. voltage at different Frequencies .....	23

## **TABLES**

Table 1: Laser Parameters and corresponding values	19
Table 2: Table showing velocity of laser powered and Pristine wire at different laser power	21

# Chapter 1

## Introduction

---

### 1.1. Bio-inspired Soft Robotics

Before we explore soft robotics, let us make sure we understand what robotics is all about. Robotics is the discipline focused on developing machines with the essential abilities for movement, perception, and cognition, based on predetermined specifications. Using robotics, machines can perform tasks like those carried out by humans or animals. The original concept of robotics involved studying how humans or animals work, like their bodies, muscles, and nerves, and then copying those functions into machines[1]. These machines were designed to be similar in shape to humans or animals and perform tasks with more strength, speed, and accuracy. Yet, there is still a tricky line between robots and humans because today's robots need precise control[2]. While they are great at doing the same tasks over and over in factories, they have trouble dealing with unpredictable situations. One major problem with these robots is that they are not good at collaborating with people. This means they can't safely work near humans or fragile objects[1]. They are usually big, heavy, and move quickly, exerting a lot of force. Plus, they often handle dangerous tools like welding or metal-cutting equipment. So, it's risky for them to be close to humans. Soft robotics stands out as a great solution for this challenge. Soft robotics represents a shift from traditional robots with rigid structures to bio-inspired continuum robots[3]. These new robots are naturally flexible and can stretch considerably as they perform their tasks. Soft robots are quite significant, even at this early stage of their development. They have the ability to overcome some of the limitations of traditional hard robots and tackle challenges that hard robots cannot handle. They can bend and mold to curved and uneven surfaces. Soft robots utilize highly flexible materials like polymers, rubbers, silicones, and other elastomers for both their main structure and moving components[4]. These materials can undergo substantial deformations while maintaining their structural integrity. Production techniques like 3D printing or molding are commonly used to fabricate these robots, allowing for the creation of complex shapes and structures. Even though these materials aren't as stiff as the metals used in hard robots, soft robots offer more flexibility and adjustability in the workspace[5]. This makes the working area safer, especially when humans and robots are working together. The significance of soft body parts becomes evident when we observe various natural organisms. Softness, flexibility and the ability to think through actions are advantageous traits that simplify how these organisms control their

behavior. In fact, the majority of natural organisms are soft-bodied, and even those with rigid skeletons are primarily composed of soft materials. Creatures such as caterpillars, octopuses, manta rays, certain fish, snakes, birds, plants, and more, have given engineers ideas for making new soft technologies and systems[6]. They have also sparked innovation in how we move on land, underwater, and through the air.

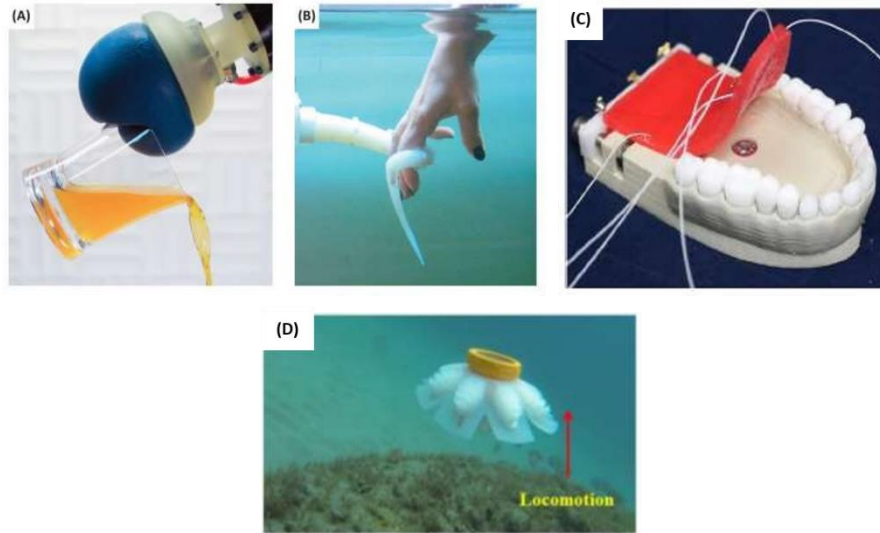


**Figure 1:** (a) A soft robotic gripper. (b) A soft manipulator modeled on the characteristic muscle structure of the octopus. (c) SMA wire embedded tongue. (d) Hydraulic based soft robotic jellyfish.

Soft robots usually use silicone or rubber because they need to move in a flexible way. But sometimes, they use special flexible plastics called elastomeric polymers to be even more flexible, especially in robots with many ways of moving. Another material that is often used is called SMA, which stands for shape memory alloy. SMA is chosen because regular electric motors don't work well in soft robots, so SMA is used to make them move instead. Soft robots possess unique features and advantages, making them applicable in various fields. From industrial to medical sectors, soft robots find diverse uses.

## 1.2. Shape Memory Alloy

Shape memory alloy (SMA), a smart material activated by heat finds extensive application in soft actuators and bioinspired robots. SMAs belong to a group of materials capable of deformation and reverting to their original "memorized" shape through loading/thermal cycles, owing to their inherent ability to undergo reversible changes in the crystal structure. SMAs can take on various shapes such as rods, plates, ribbons, springs, and wires, allowing for direct actuation on a small scale. SMAs made from iron or copper, such as Fe—Mn—Si,

Cu–Zn–Al, and Cu–Al–Ni, are often chosen because they are inexpensive and easy to find[5]. However, NiTi-based SMAs are generally preferred for most applications due to their greater stability and practicality. The functioning of SMA actuators, irrespective of their form, relies on the martensite versus austenite phase transitions of SMAs. This poses certain limitations, such as low actuation frequency and challenges in precise control, as these phase transitions are temperature-dependent.

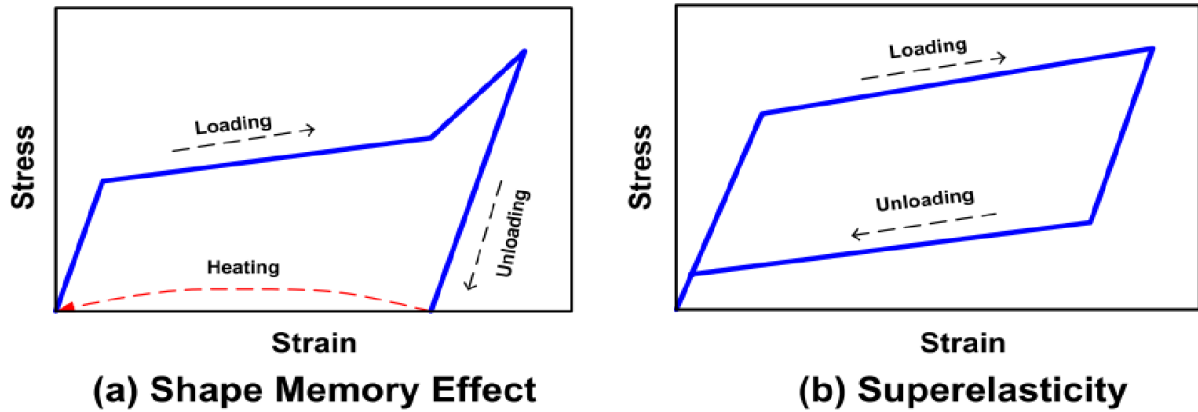


*Figure 2: (a) Shape memory effect. (b) Super-elasticity*

### 1.3. Polydimethylsiloxane (PDMS)

PDMS is available in the form of PDMS A and PDMS B (Resin and Hardener). PDMS A and B are mixed in a 10:1 ratio and stirred thoroughly to avoid air bubbles. Additionally, the mixture is placed inside a vacuum chamber to remove any remaining air bubbles completely, as shown in Figure 3. The mixed PDMS solution is then poured into the mold (a 3D-printed structure), and the SMA wire is properly positioned. After pouring, the structure is cured at 55°C for 7 hours. Once cured, the SMA-embedded PDMS soft actuator is removed from the mold.

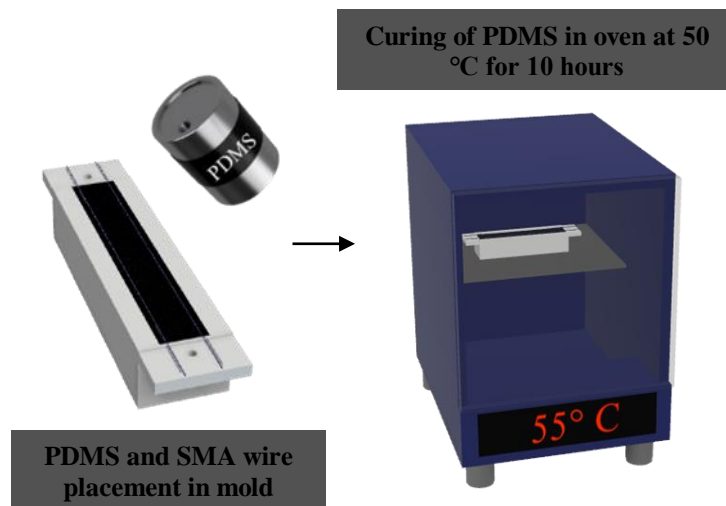


*Figure 3: PDMS pouring and curing the composite into the oven*

### 1.4. 3-D Printing of Mold Structure

The mold needed for curing the PDMS is made using a 3D printer. The mold is usually made of PLA material. First, the design of the mold is created using modeling software, and then it is sliced using CURA software. This slicing process converts the design into x, y, and z coordinates. The mold is then printed with the 3D printer, and the time it takes depends on the size and volume of the mold.

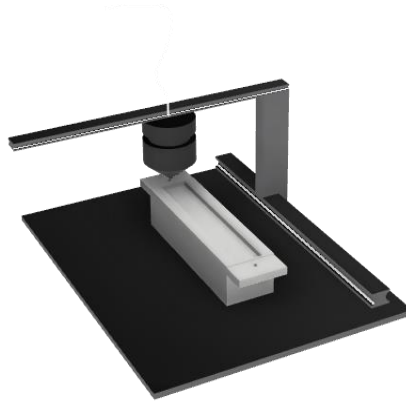


*Figure 4: 3-D Printed Mold Structure*

### 1.5. Outline of the thesis

**Chapter 1:** Introduction

**Chapter 2:** Literature Review

**Chapter 3:** Laser Anchoring and Laser Parameters

**Chapter 4:** Fabrication of Laser-Anchored SMA-PDMS Structure

**Chapter 5:** Results and Discussions

## Chapter 2

### Literature Review

---

Hyung et al. developed a biomimetic swimming robot inspired by the locomotion of a marine turtle. This robot achieved bending and twisting movements using a smart soft composite (SSC), where passive materials played a crucial role. The actuator's posterior positive angle was realized by offsetting the SMA wire on the topside of the actuator. The fabricated flipper, measuring 64.3 mm in length, demonstrated a bending of 55 mm and a twisting angle of  $24^\circ$ . This robot achieved a swimming speed of 22.5 mm/s.

Song et al. created a biomimetic turtle flipper actuator using an SMA composite structure, intended for an autonomous underwater vehicle inspired by a turtle. They measured the generated thrust and swimming efficiency in different swimming gaits of the flipper actuator. Their findings showed that while the vigorous gait produced higher thrust, it had relatively lower swimming efficiency compared to the routine gait. The flipper actuator, when implemented in a biomimetic turtle robot, achieved a maximum swimming speed of 11.5 mm/s in the vigorous gait[7].

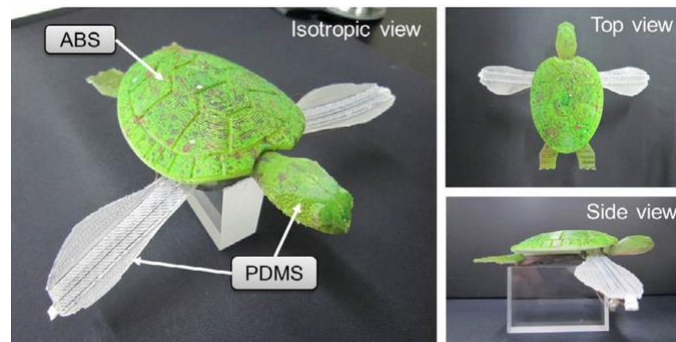


***Figure 5 Turtle-based actuator using a composite structure***

Conventional turtle-like robot actuators face size and weight limitations, and replicating the soft deformed movements of biological organisms is challenging due to the linkage systems in rigid structures. The SSC actuators developed for the turtle robot provide an effective solution to these issues.

An inchworm-inspired biomimetic robot was developed by Wang et al. using an SMA composite structure capable of both linear and turning locomotion. The composite structure, comprising SMA wires, was used to replicate the longitudinal fibers of the inchworm, while PDMS provided the body due to its softness, isotropic properties, and better adhesion with SMA wires. The robot achieved a linear speed of 3.6 mm/s and a stride length of 54 mm, making it suitable for remote rescue and

reconnaissance missions where access by humans or larger robots is not possible. Another inchworm robot, developed with SMA and glass fiber reinforced polymer strips by Kim, demonstrated unidirectional movement, covering 4 mm over a given period.

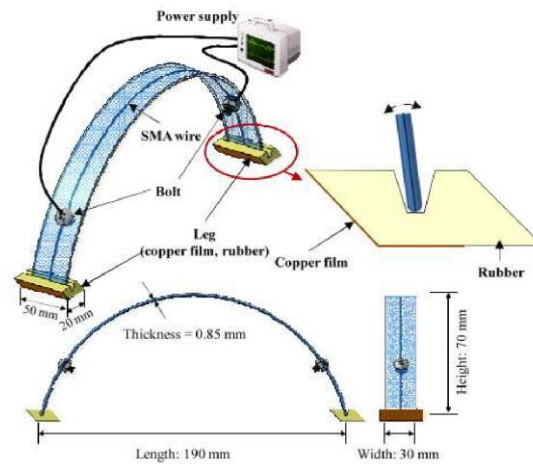


**Figure 6: SMA wire/GFRP composite-based inchworm robots**

Later, the same research group developed an SMA-embedded soft morphing structure with substantial thickness and deformation capabilities. The skeleton material was ABS, a stiff thermoplastic polymer commonly used in structural applications. The performance evaluation of the prototype revealed significant actuation and force generation, suggesting potential applications such as cell phone robots that exhibit crawling motion.

Seok et al. developed a multi-segmented soft robotic platform called Meshworm, which performs peristaltic locomotion using an SMA and mesh tube structure. Each segment operates as a stretched coil spring, and the addition of multiple longitudinal muscles distributed along the circumference allows the robot to navigate three-dimensional spaces, overcoming large obstacles and rough terrain[8].

Tomodachi et al. utilized SMA coils and motor tendons to develop soft robotic worms. These robots, rapidly produced using 3D printing, exhibited crawling and steering capabilities, demonstrating simple yet effective approaches to controlling highly deformable robots.

Villanueva et al. introduced Robojelly, a robotic jellyfish with SMA-based BISMALC actuators. These actuators, composed of silicone, SMA wires, and spring steel, enabled Robojelly to produce enough thrust for propulsion, achieving a proficiency of  $0.19 \text{ s}^{-1}$ , comparable to the natural medusa's  $0.25 \text{ s}^{-1}$ . However, a folding effect in the silicone bell was observed, reducing performance[9].

Koet al. developed a jellyfish-mimicking robot controlled by an external magnetic field generated

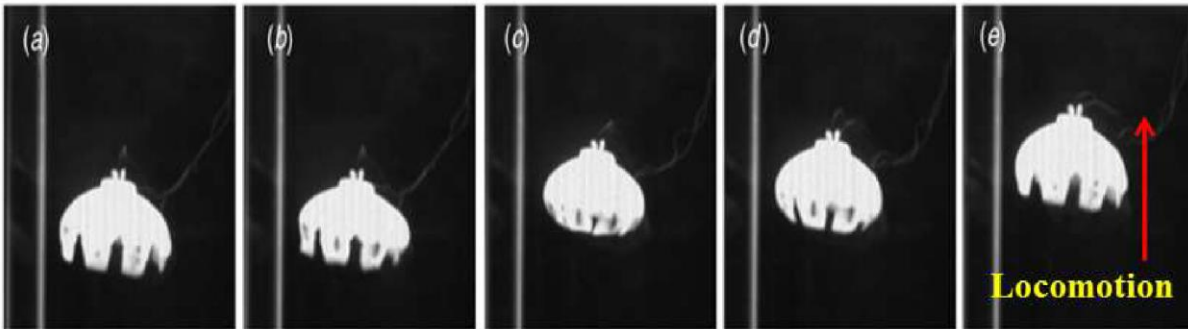


**Figure 7: BISMAL-based Robojelly**

by Helmholtz coils. Through various tests, they determined that a 10 Hz square-type waveform was optimal for the EMA system's actuating input current. The robot demonstrated 3D locomotion using a 3 Hz square input current[10].

Yeom et al. fabricated a biomimetic jellyfish robot using ionic polymer metal composite actuators, designed to mimic the real locomotion of jellyfish with pulse and recovery processes. The bio-inspired input signal, replicating the jellyfish's natural movements, induced significant vertical displacement, enhancing the robot's floating capability[11].

Xiao et al. developed a self-propelled jellyfish robot using a six-bar linkage mechanism, with a rigid head and hull made of ABS material. The robot, centrally symmetric with four actuators, successfully achieved swimming motion by controlling these actuators. Another jellyfish robot, made with white nylon and hollow molding for the barycentre mechanism, achieved an average swimming speed of 100 mm/s[12].

Godaba et al. introduced a jellyfish robot with a dielectric elastomer actuator, consisting of a bell,

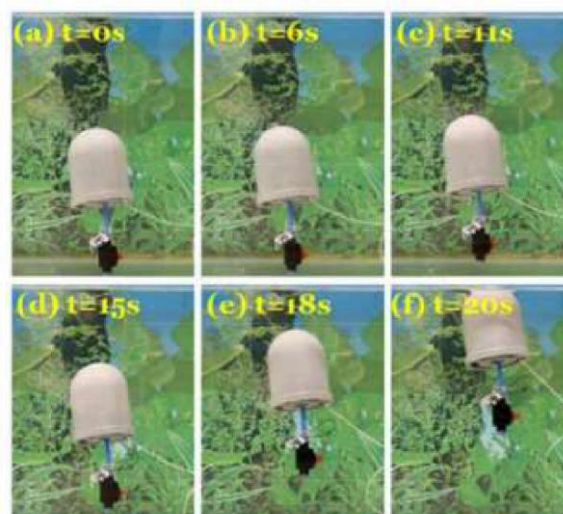


**Figure 8: Dielectric elastomer-based jellyfish**



an air chamber, and a dielectric elastomer membrane. The actuator, subjected to voltage, expanded the membrane, increasing the volume of air and the buoyant force. This mechanism allowed the robot to propel itself by ejecting water, demonstrating effective underwater movement.

Frame et al. developed soft robotic jellyfish using hydraulic network actuators, with each tentacle having a common channel connected to an impeller pump. These silicon rubber actuators allowed the jellyfish to swim through narrow orifices and navigate directionally by offsetting tentacle actuation strokes. Tested in the ocean, these robots showed potential for monitoring delicate ecosystems without causing damage[13].

Cho et al. developed a body caudal fin propulsion system using an SMA spring actuator mounted on a flexure-based frame. The SMA spring-driven caudal fin achieved undulatory motion by actuating in succession, creating a sequence of shapes to mimic a fish's natural movement. This design, with varying segment lengths, improved the realism and efficiency of the tail motion[14].

Wang et al. developed a wireless microrobot manta ray using SMA wire-actuated oscillating pectoral fins. The fins, made of polyvinyl chloride (PVC) sheet, allowed the microrobot to achieve a maximum swimming speed of 57 mm/s and a maximum amplitude of 40 mm[15].

Ravalli et al. created a bio-inspired fish robot equipped with polycarbonate electrochemical sensors to detect hydrogen ions and transform them into electronic signals for robot control. This proof-of-concept for multi-sensor fish robots aims to provide early information on environmental changes, improving farm management and fish well-being[16].

Wang et al. developed a micro-robot fish with a biomimetic fin structure inspired by squid/cuttlefish fins. The fin, made of an elastic substrate, skin, and SMA wires, allowed for forward and turning swimming movements. The micro-robot achieved a maximum swimming speed of 112 mm/s and a minimum turning radius of 136 mm.

McGovern et al. investigated the thrust force generated by polypyrrole trilayer actuators in fish-like robots, providing valuable insights into optimizing polymer actuators for maximum swimming speeds.

Rossi et al. explored bio-inspired locomotion for underwater robots, using bendable structures and SMA-based actuation muscles to improve maneuverability. Their prototype used SMA actuators to bend a flexible polycarbonate backbone, supported by ribs and a silicon-based skin for a three-dimensional shape.

# Chapter 3

## Laser Anchoring and Laser Parameters

---

### 3.1. Laser Anchoring

Laser anchoring is a sophisticated technique employed to create stable and controlled modifications on the surface of materials through the precise application of laser irradiation. This method proves exceptionally beneficial for manipulating the physical properties of materials, such as shape memory alloys (SMAs), by inducing localized changes. By meticulously directing laser energy to specific areas, we can cause microstructural alterations that significantly enhance the performance and functionality of these materials. This precision makes laser anchoring indispensable for applications requiring exact property control, including actuators, sensors, and biomedical devices.

In our project, we utilized laser anchoring to alter the surface characteristics of SMA wires. The process commenced with the careful calibration of laser parameters—such as beam profile, laser power, duration, pulse width, mark speed, and beam diameter—to achieve the desired modifications while preserving the material's integrity. By applying the laser to targeted regions of the SMA wires, we induced localized heating and subsequent microstructural changes. These modifications aimed to enhance the material's performance in specific applications, ensuring that the SMA wires adhered to the stringent requirements of high-precision devices.

We employ laser anchoring because when a laser irradiates a shape memory alloy (SMA), it creates precise markings on its surface. These markings enhance the adhesion of the SMA to polydimethylsiloxane (PDMS), significantly improving the material's actuation performance. The increased surface roughness from the laser-induced markings reduces slipping between the SMA and PDMS by increasing friction. This enhanced friction ensures a more reliable and efficient actuation, which is crucial for applications requiring precise movement and control.

### 3.2. Laser Parameters

In our study, precise calibration of laser parameters was essential to achieve the desired surface modifications of the NiTi shape memory alloy (SMA) wires without compromising their structural integrity. The beam profile utilized was a Gaussian beam, known for its ability to focus energy precisely and create uniform modifications. The laser power was varied at four different levels: 12 W, 15 W, 17.5 W, and 20 W, allowing us to observe the effects of different energy intensities on the SMA wires. A pulse width of 25 microseconds was selected to control the duration of laser

exposure, balancing the need for effective energy delivery and minimizing thermal damage. The marking speed was set at 1 Bits/ms, ensuring a consistent application of the laser over the targeted areas. Lastly, a beam diameter of 50 microns was chosen to achieve a fine focus, enabling precise and localized modifications. These carefully calibrated parameters played a crucial role in optimizing the laser anchoring process, and enhancing the adhesion and actuation performance of the SMA-PDMS structures.

Parameters	Value/Comments
Beam Profile	Gaussian Beam
Laser Power	12 W, 15 W, 17.5 W, 20 W
Pulse Width	25 microseconds
Mark Speed	1 Bits/ ms
Beam Diameter	50 microns

*Table 1: Laser Parameters and corresponding values*

### 3.3. Laser Anchoring on 0.5 mm NiTi Wire

In our investigation, we performed laser anchoring on 0.5 mm diameter NiTi shape memory alloy (SMA) wires to study the effects of various laser power settings on the surface characteristics. Following the laser treatment, surface profilometry was conducted to analyze the modifications. At a laser power of 12 watts, we observed extremely low marking, indicating insufficient energy to induce significant surface changes. Conversely, at a laser power of 22 watts, the wire experienced failure, demonstrating that excessive energy input can compromise the material's structural integrity.

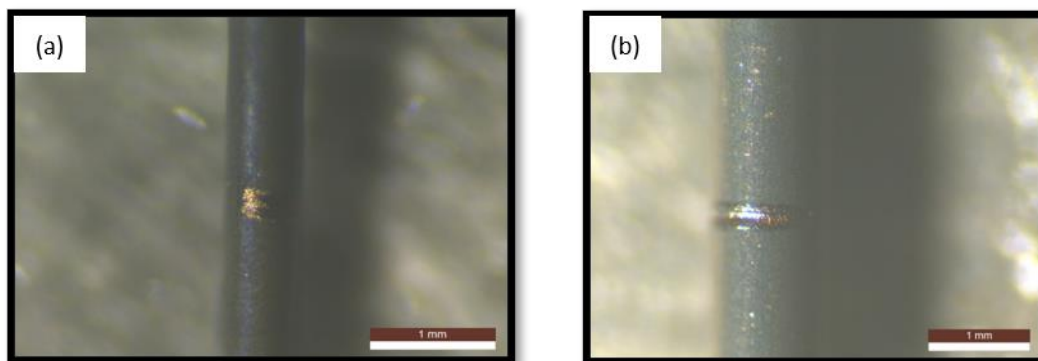


*Figure 9:(a) Laser anchoring using laser power 12 watt. (b) Laser anchoring using laser power 22 watt*

To optimize the process, we selected two intermediate power levels: 15 watts and 20 watts. Surface

profilometry of the samples treated at these power levels revealed distinct surface modifications. At 15 watts, a filler was observed on the wire surface, which resulted from the solidification of material due to the laser's localized heating effect. The filler height was measured at 23.3 microns, indicating a substantial alteration that could enhance the bonding surface for PDMS. At 20 watts, a crater formation was observed, with a depth of 5.7 microns, showing a different type of surface modification caused by the increased energy. These findings highlight the importance of carefully selecting laser power settings to achieve the desired surface characteristics while maintaining the material's integrity for improved performance in actuation applications.

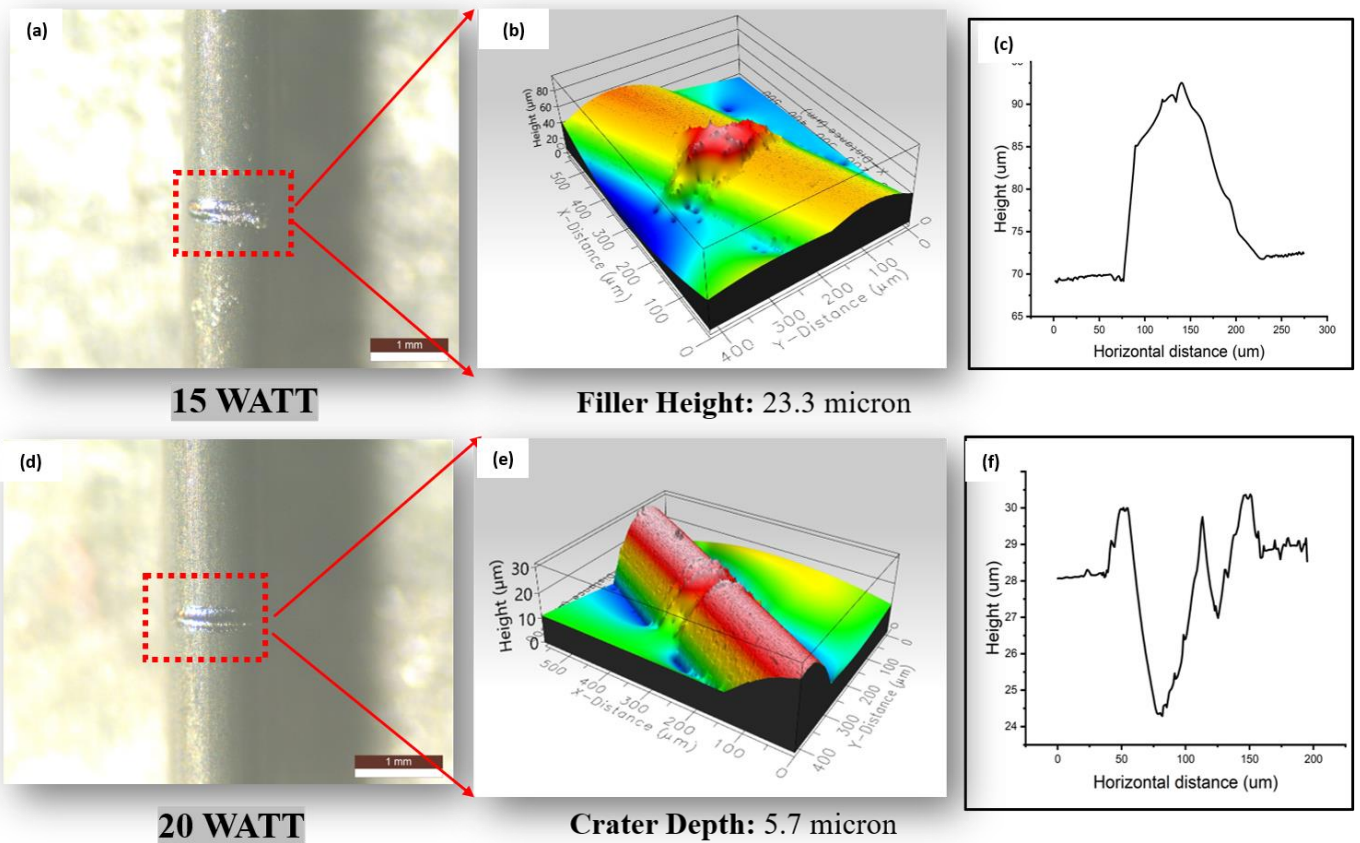


**Figure 10:**(a) &(d)Optical image with laser power 15 and 20 watts respectively. (b)&(e) Surface profilometry with laser power 15 and 20 watts respectively. (c)&(f)graph Height vs Horizontal distance.

### 3.4. Actuation of Anchored and Pristine Wire

Following the surface modifications achieved through laser anchoring, we conducted actuation tests on both anchored and pristine NiTi wires to evaluate their performance. Interestingly, the pristine wires demonstrated superior actuation results compared to the laser-anchored wires. This discrepancy can be attributed to the increased stiffness introduced by the laser anchoring process. The microstructural changes induced by the laser energy, while beneficial for enhancing surface adhesion, inadvertently increased the wire's rigidity. Consequently, to achieve the desired actuation,

we had to perform manual bending of the laser-anchored wires, which significantly extended the actuation time. The increased stiffness created a resistance that the wires had to overcome, leading to slower response times.

Power	Voltage	Current	Displacement	Time	Velocity
Pristine SMA	0.6 V	1.28 A	75 mm	13 sec	5.77 cm/sec
15 Watt	0.6 V	0.8 A	75 mm	58 sec	1.29 cm/sec
20 Watt	0.6 V	0.7 A	70 mm	80 sec	0.87 cm/sec
22.5 Watt	0.6 V	0.9 A	60 mm	14 sec	4.28 cm/sec

**Table 2: Table showing velocity of laser powered and Pristine wire at different laser power**

### 3.5. Laser Anchoring on 0.25 mm NiTi Wire

To address the challenges observed with the 0.5 mm diameter NiTi wires, particularly the increased stiffness and potential for PDMS peel-off due to higher actuation forces, we conducted laser anchoring on 0.25 mm diameter NiTi wires. The rationale behind this adjustment was based on the prediction that the integration of 0.5 mm wires, which require higher power for actuation, could lead to the detachment of the PDMS matrix due to the larger forces involved. By using 0.25 mm wires, we aimed to create a more suitable structure that balances actuation performance and material integrity.

Following a similar procedure as with the 0.5 mm wires, we carefully calibrated the laser parameters and performed surface profilometry on the modified wires. At a laser power of 20 watts, we observed failure of the 0.25 mm wires, indicating that this power level was too high and compromised the wire's structural integrity. Consequently, we focused on two intermediate power settings: 15 watts and 17.5 watts. The profilometry results revealed distinct surface modifications for these power levels. At 15 watts, we observed a crater depth of 2 microns, indicating a moderate level of surface alteration. At 17.5 watts, a filler height of 18 microns was observed, resulting from the solidification of material induced by the laser's localized heating. These surface characteristics were similar to those observed in the 0.5 mm wires but adjusted for the reduced wire diameter, ensuring a better integration with the PDMS matrix and potentially enhancing the overall actuation performance of the composite structure.

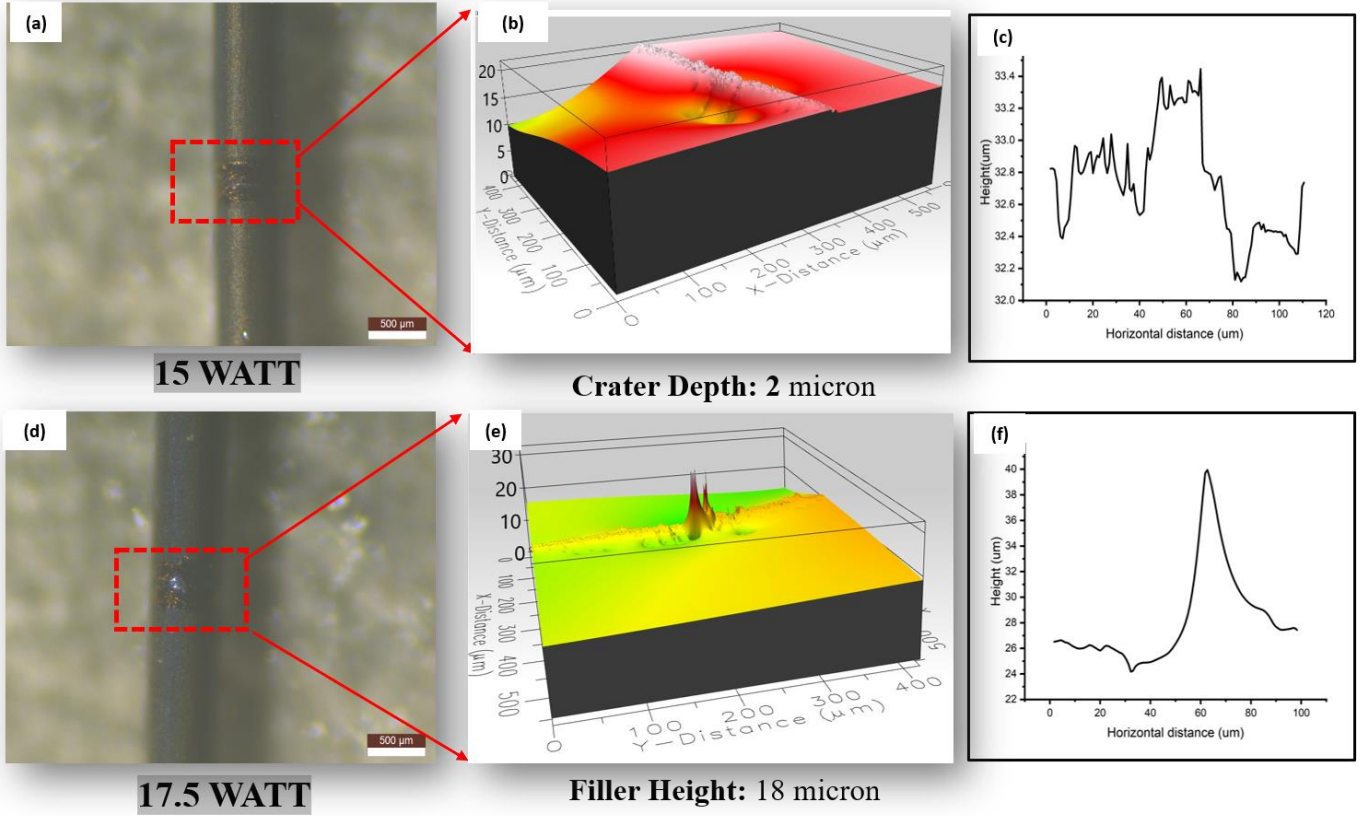


**Figure 11:**(a) &(d)Optical image with laser power 15 and 17.5 watts respectively. (b)&(e) surface profilometry with laser power 15 and 17.5 watts respectively. (c)&(f)graph Height vs Horizontal distance.

### 3.6. Summary

In this chapter, we conducted laser anchoring on 0.5 mm diameter NiTi shape memory alloy (SMA) wires to examine the effects of various laser power settings on the surface characteristics. Surface profilometry was employed following the laser treatment to analyze these modifications. At a laser power of 12 watts, extremely low marking was observed, indicating that the energy was insufficient to induce significant surface changes. Conversely, at a power of 22 watts, the wire experienced failure, demonstrating that excessive energy compromised the material's structural integrity. To optimize the process, we selected two intermediate power levels: 15 watts and 20 watts. Profilometry of the samples treated at these power levels revealed distinct surface modifications: a filler height of 23.3 microns at 15 watts due to the solidification of material from localized heating, and a crater depth of 5.7 microns at 20 watts, showing a different type of surface alteration.

Subsequently, we performed actuation tests on both anchored and pristine wires. The pristine wires exhibited superior actuation results, as the increased stiffness from laser anchoring required manual bending, prolonging actuation time. However, we predicted that integrating the SMA wires with PDMS would

enhance actuation performance by reducing slippage and increasing friction at the interface. To address the potential issue of PDMS peel-off with 0.5 mm wires due to higher forces, we conducted laser anchoring on 0.25 mm diameter wires. At 20 watts, these wires failed, so we focused on 15 watts and 17.5 watts. At 15 watts, a crater depth of 2 microns was observed, while at 17.5 watts, a filler height of 18 microns was noted. These adjustments ensured better integration with the PDMS matrix, aiming to balance actuation performance and material integrity for improved underwater soft robotics applications.

# Chapter 4

## Fabrication of Laser Anchored SMA-PDMS Structure

---

### 4.1. Analytical Model

To predict the configuration of the soft actuator, a free-body diagram of the wire is illustrated in Figure 10, showcasing the analytical model.

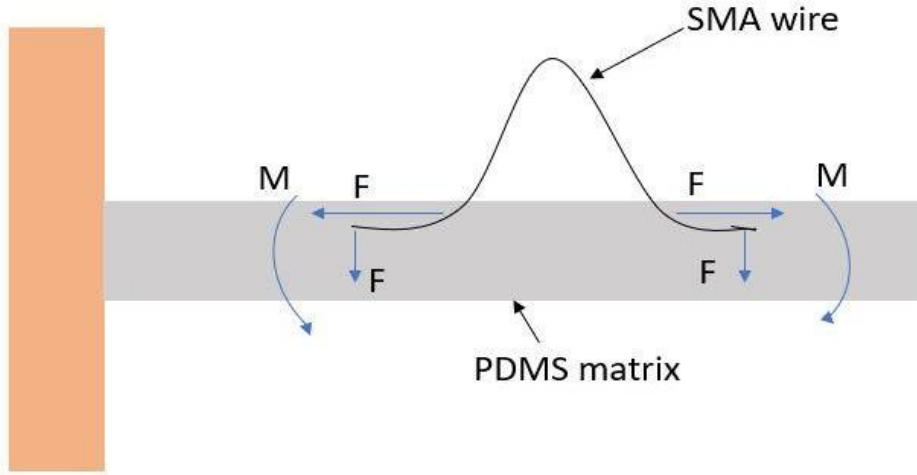


*Figure 12: Analytical Model*

In this model, the NiTi SMA wire is embedded in a flexible PDMS structure in a hump configuration. When heated, the SMA wire tends to straighten, generating bidirectional forces  $F_x$  and  $F_y$  at the wire ends. These forces produce a bending moment ( $M$ ) around the  $z$ -axis, which passes through the wire's center. This bending moment results in the actuator bending in one direction during joule heating. For achieving two-way actuation, the wire in the hump configuration must be embedded in both directions, allowing for bidirectional bending motion.

### 4.2. Fabrication Process

The actuator was fabricated through the Shape Deposition Manufacturing (SDM) process, which involves several meticulous steps to ensure the creation of a high-quality, functional actuator.

#### PDMS Solution Preparation Process

- I. **Mixing the base and binder:** The first step involved preparing the PDMS solution by taking the base polymer and the binder in a precise ratio of 10:1. These components were manually mixed for 5 minutes to ensure thorough blending. The manual mixing process is crucial to achieving a homogeneous solution that will provide consistent properties in the



final product.

- II. **Degassing the Mixture:** After mixing, the PDMS solution was subjected to a vacuum curing process to eliminate any intrinsic bubbles that may have formed during mixing.

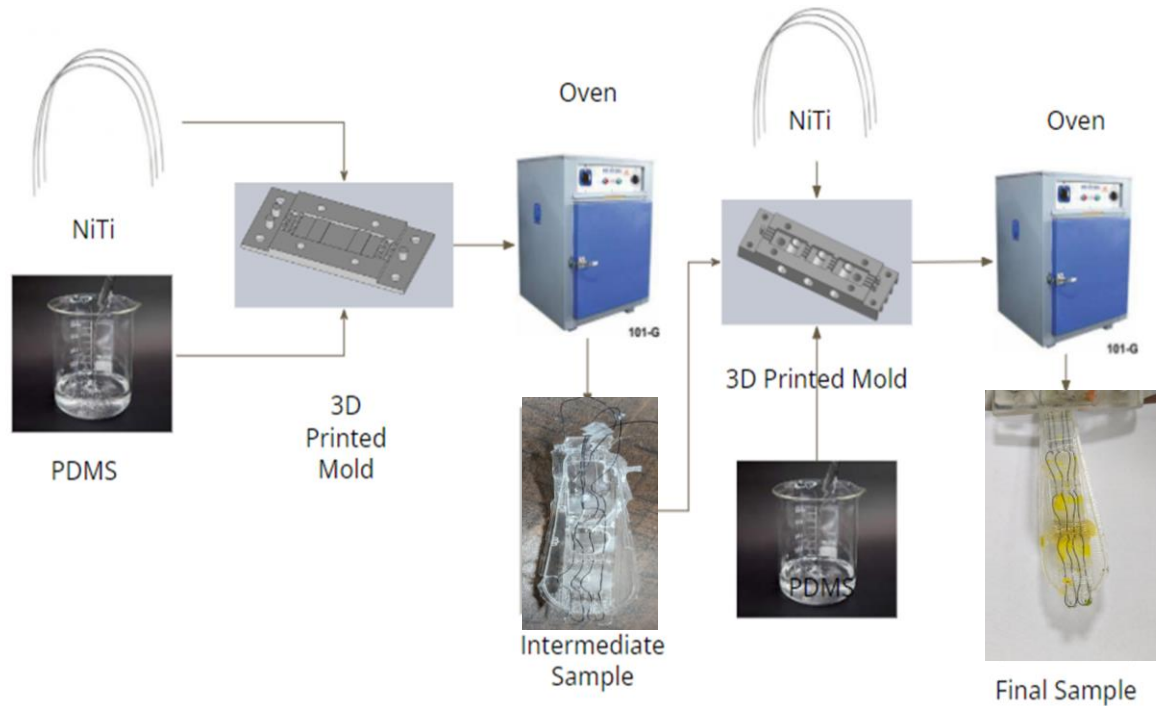


**Figure 13: Shape Deposition Manufacturing**

This degassing step is essential to prevent the formation of voids or weak points in the cured PDMS, which could compromise the structural integrity and performance of the actuator.

### Actuator Fabrication Process

- I. **Fixing the NiTi Wire in the Mold:** The NiTi wire was carefully fixed into a specially designed 3D printed mold. This mold contained cavities specifically shaped to accommodate the curvature of the wire's hump geometry. Precise placement of the wire was critical to ensure that the desired humped shape was achieved, which is necessary for the actuator's intended functionality.
- II. **Pouring the PDMS into the Mold:** Once the wire was securely positioned, the mold was closed to create a sealed environment. PDMS was then poured into the mold, ensuring that it filled all cavities and encapsulated the NiTi wire completely. This step required careful handling to avoid introducing air bubbles or gaps within the mold.
- III. **Initial Curing of the PDMS:** The mold containing the PDMS and NiTi wire was placed in an oven and cured at 55 °C for 7 hours. This initial curing step solidified the PDMS, forming

an intermediate sample. The controlled temperature and curing duration were critical to achieving the desired mechanical properties and ensuring proper embedding of the wire within the PDMS matrix.

- IV. **Peeling Off the Intermediate Sample:** After the initial curing and cooling, the intermediate sample was carefully peeled off from the mold. This step required precision to avoid damaging the partially formed actuator and to ensure that the wire remained properly embedded in the PDMS.
- V. **Sealing the Intermediate Sample in the Second Mold:** The intermediate sample was then placed into a second 3D printed mold designed to accommodate the next stage of the fabrication process. Any gaps in the mold were meticulously sealed to prevent leakage of PDMS during the subsequent heating cycle. Ensuring a tight seal was crucial for maintaining the integrity and shape of the final actuator.
- VI. **Final Curing:** The sealed mold containing the intermediate sample was reheated in the oven at 55 °C for an additional 7 hours. This second curing step further solidified the PDMS and finalized the actuator's structure. The controlled reheating process ensured that the PDMS fully adhered to the NiTi wire, creating a robust and reliable actuator.

By following these detailed steps, we successfully fabricated an actuator with the desired properties and performance characteristics suitable for underwater soft robotics applications.

### **4.3. Double-layer clay cover molding**

In this sophisticated molding process, the SMA wire is meticulously fixed inside the grooves using screws. This initial step is crucial to ensure the precise positioning and alignment of the wire. After securing the wire, the remaining portions of the grooves are filled with clay to provide additional support and stability during the molding process. To prevent any adverse interactions between the PDMS and clay—which could potentially alter the properties of the PDMS—a thin PLA sheet is placed over the clay. This protective layer ensures that the PDMS does not come into direct contact with the clay, maintaining its intended material characteristics.

Once the clay is covered, the SMA wire is tensioned by securing it with nuts and bolts at both ends. This tensioning is essential for achieving the desired mechanical properties and ensuring that the wire remains in the correct position during the entire molding and curing process. A similar setup is prepared on a second mold to mirror the configuration. The two molds are then carefully aligned and attached using screws to create a unified mold assembly.

PDMS is then poured into the mold through specifically designed holes, ensuring that it fills all cavities and encapsulates the SMA wire completely. The filled mold is then placed in an oven and cured at a controlled temperature for 7 hours. This curing step is vital as it solidifies the PDMS, embedding the SMA wire firmly within the flexible matrix.

After the curing process is complete, the first ends of the wires are carefully released to begin the demolding process. The screws holding the molds together are then removed, allowing the molds to be gently separated. This step requires precision to avoid damaging the newly formed actuator. Finally, the actuator is peeled off from the mold, revealing a finely crafted SMA-PDMS composite structure.

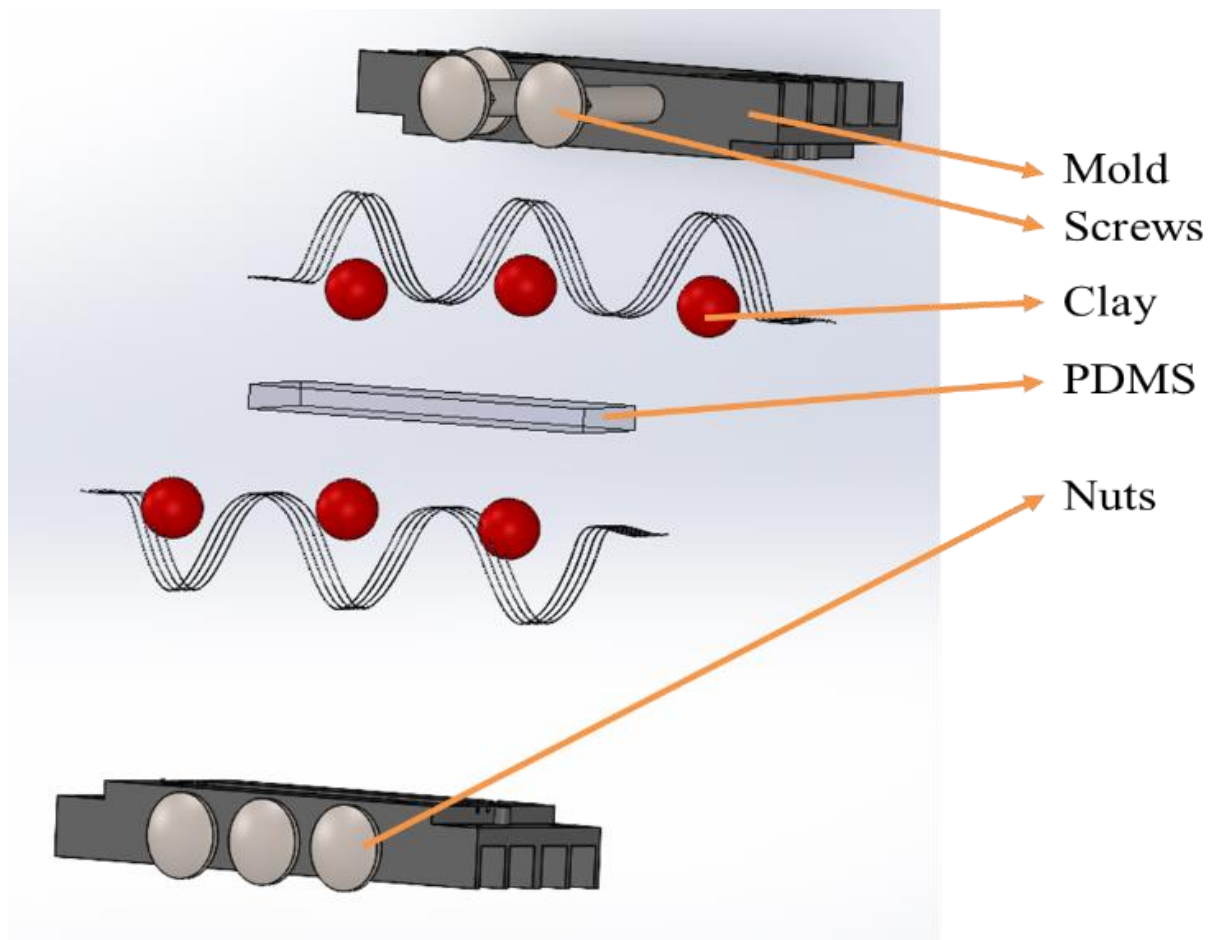


*Figure 14:Double-layer clay cover molding*

### **Advantages**

- I. This method ensures excellent dimensional accuracy, significantly reducing the chances of errors. The precision achieved through this process is essential for the reliable performance of the actuator in its intended applications.
- II. The overall time required for the process is relatively short, taking only 7 hours for curing. This single-step curing process enhances efficiency and reduces the production time.

## Disadvantages

- I. The fixing and peeling processes are complex and require careful handling. Ensuring that the SMA wire is correctly tensioned and that the molds are properly aligned demands attention to detail and precision. The demolding process, in particular, needs to be conducted meticulously to prevent any damage to the actuator.

### 4.4. Setup for electrical actuation

To evaluate the performance of the fabricated actuator, we established an electrical actuation setup. This system comprised several key components: a DC power source, an Arduino Uno microcontroller, a personal computer (PC), and the actuator sample.

The DC power source provided the necessary voltage and current to actuate the NiTi SMA wire. This power source was crucial for supplying consistent and controllable electrical energy, enabling the SMA wire to heat and undergo its shape memory transition.

The Arduino Uno served as the control unit for the actuation system. Programmed to regulate the power supplied to the SMA wire, the Arduino ensured precise control over the heating and cooling cycles. This microcontroller was integral to automating the actuation process, ensuring that the results were consistent and repeatable.

A personal computer was connected to the Arduino Uno, offering a user interface for monitoring and controlling the actuation process. Custom software on the PC facilitated real-time data acquisition and analysis, providing detailed insights into the actuator's performance. This setup allowed for comprehensive monitoring of parameters such as voltage, current, and displacement

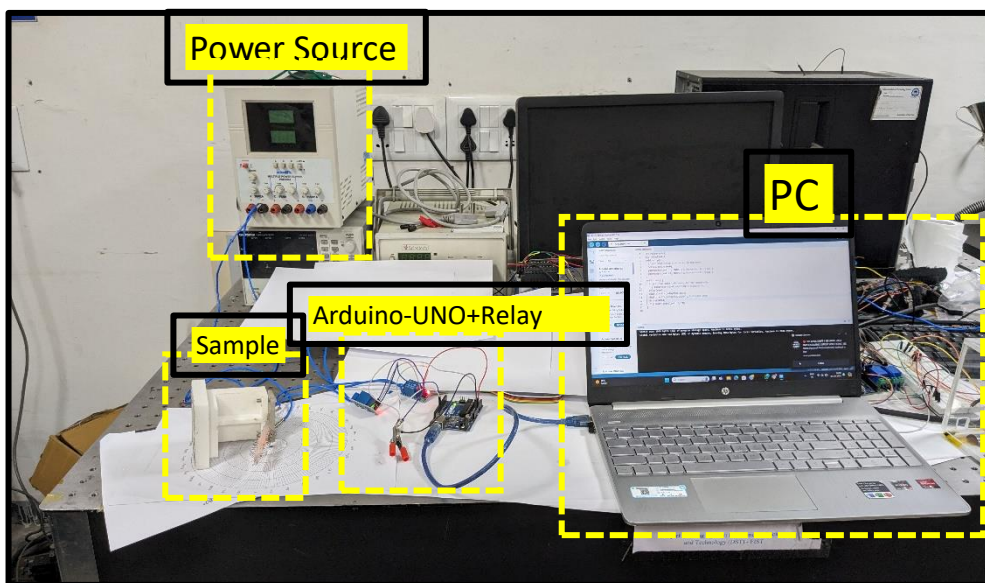


*Figure 15: Setup for Electrical Actuation*

during the actuation cycles.

The fabricated SMA-PDMS actuator was integrated into this electrical circuit. The ends of the NiTi SMA wire were securely connected to the power source, allowing current to flow through the wire and induce the shape memory effect, resulting in the desired bending motion of the actuator.

To set up the system, the DC power source was connected to the Arduino Uno, which was then linked to the PC via a USB cable. The actuator sample was carefully attached to the circuit, ensuring that the electrical connections at both ends of the SMA wire were secure. The Arduino was programmed with a custom script designed to modulate the power supplied to the wire, allowing precise control over the timing and intensity of the actuation.

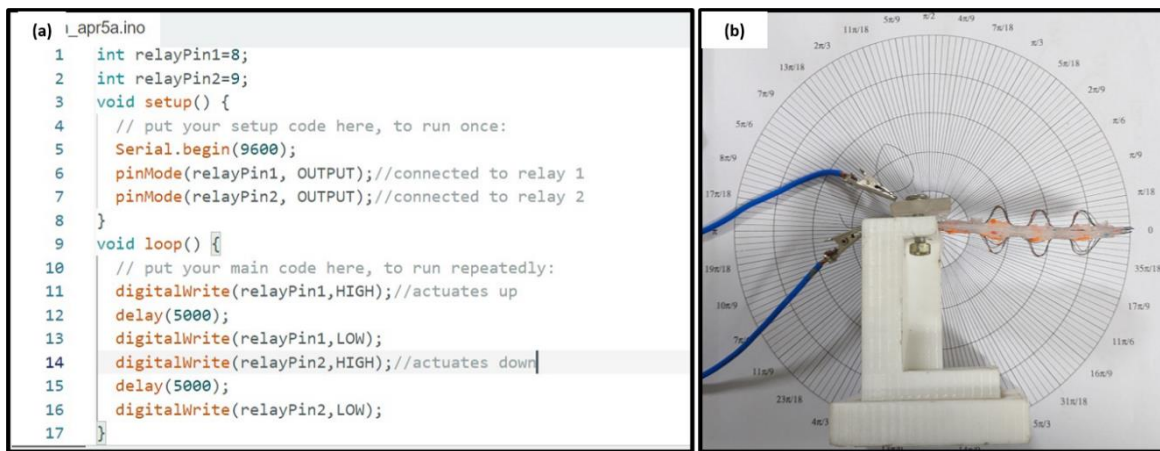


**Figure 16:(a) Source code for actuation. (b)Top view of the SMA-PDMS Structure**

## 4.5. Summary

In this chapter, we detailed the fabrication process of integrating laser-anchored NiTi shape memory alloy (SMA) wires with polydimethylsiloxane (PDMS) to create a robust actuator for underwater soft robotics. The process began with the preparation of the PDMS solution by mixing the base and binder, followed by degassing to remove air bubbles. The NiTi wire was then carefully positioned in a 3D-printed mold and encapsulated with PDMS. The assembly underwent a two-step curing process: an initial 7-hour cure at 55 °C to form an intermediate sample, followed by a second 7-hour cure after resealing the mold. This meticulous process ensured precise embedding of the wire, resulting in a high-quality actuator with enhanced performance and reliability. We set up an electrical actuation system to evaluate the performance of the fabricated SMA-PDMS actuator. The system included a DC power source, an Arduino Uno microcontroller, a PC, and the actuator sample

# Chapter 5

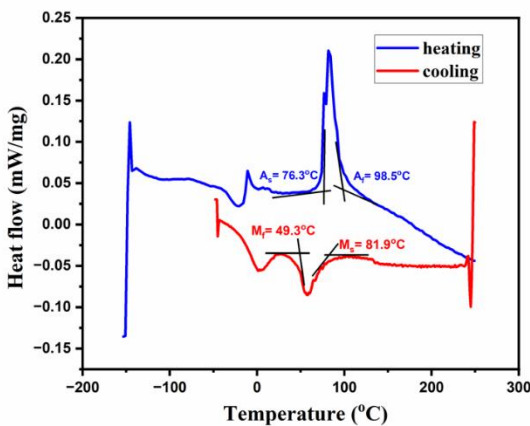
## Results and Discussion

In this chapter, we present the findings from our experiments on the laser-anchored NiTi SMA-PDMS actuators. The discussion includes a comparative analysis of the actuation performance between pristine and laser-anchored wires, with a focus on the impact of various laser parameters and the effectiveness of our fabrication and actuation processes.

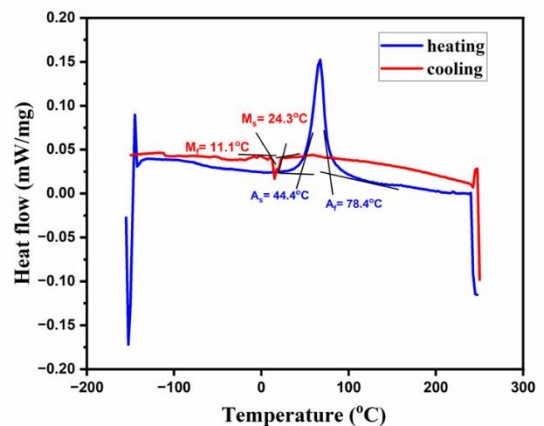
### 5.1. Phase Transformation Analysis

We conducted a phase transformation analysis using Differential Scanning Calorimetry (DSC) to compare the heating and cooling cycles of pristine and laser-anchored SMA wires. The temperature range for this analysis was set between -150°C and 250°C. Key parameters such as Austenite Start ( $A_s$ ), Austenite Finish ( $A_f$ ), Martensite Start ( $M_s$ ), and Martensite Finish ( $M_f$ ) temperatures were recorded for both cycles.

For the pristine SMA wire, during the heating cycle, the Austenite Start temperature was 79.3°C, and the Austenite Finish temperature was 98.5°C. In the cooling cycle, the Martensite Start temperature was 81.9°C, and the Martensite Finish temperature was 49.3°C. In contrast, the laser-anchored SMA wire (treated at 17.5 watts) exhibited significantly lower transformation temperatures. The Austenite Start and Finish temperatures during the heating cycle were 44.4°C and 78.4°C, respectively. During the cooling cycle, the Martensite Start and Finish temperatures were 24.3°C and 11.1°C, respectively.



Pristine NiTi wire



Anchored NiTi wire  
Laser power : 17.5 watt

*Figure 17: Graph of Heat flow vs Temperature of Pristine and Laser Anchored NiTi Wire*



The lower phase transformation temperatures in the laser-anchored wire indicate a reduced power requirement for achieving actuation. This efficiency implies that at the same power levels, the laser-anchored SMA wire will perform better than the pristine wire, providing enhanced actuation with lower energy consumption. These findings highlight the benefits of laser anchoring in optimizing the thermal and actuation properties of SMA wires, making them more efficient for applications requiring precise temperature control and lower energy usage.

### 5.2. Angular displacement and Voltage

To investigate the relationship between angular displacement and voltage, we fabricated two laser-anchored SMA samples using laser powers of 15 watts and 17.5 watts. These samples were compared with a pristine SMA wire to evaluate the differences in actuation performance. The voltage levels applied were 5 V, 5.5 V, 6 V, and 6.5 V.

At lower voltages, the pristine SMA wire exhibited better angular displacement compared to the laser-anchored samples. This result can be attributed to the increased stiffness introduced by the laser anchoring process, which initially hinders the actuation. As the voltage increased, however, the performance of the laser-anchored samples improved significantly. At higher voltages, both the 15 watt and 17.5 watt laser-anchored samples demonstrated greater angular displacement than the pristine wire.

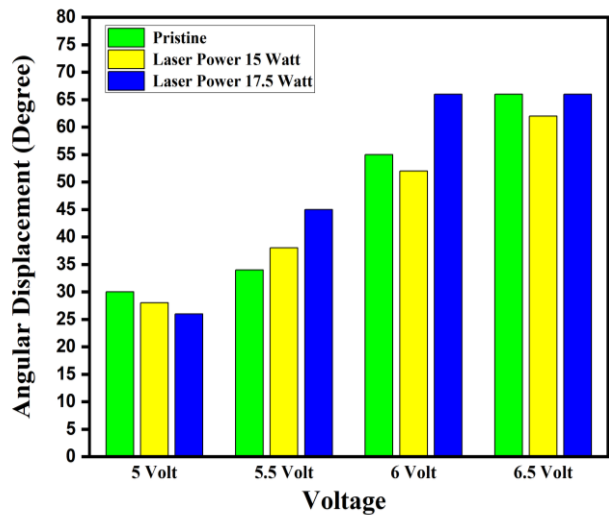


**Figure 18: Angular Displacement Vs Voltage**

The graph above illustrates this behavior, showing that while pristine wires perform better at lower voltages, the laser-anchored wires surpass them as the voltage increases. This trend suggests that the laser-anchored SMA wires are more effective at higher energy inputs, likely due to the enhanced adhesion and reduced slippage between the SMA and PDMS. This improved performance at higher

voltages makes laser-anchored wires particularly suitable for applications requiring greater actuation force and precision.

### 5.3. Angular Velocity and Voltage

In the next phase of our study, we examined the relationship between angular velocity and voltage for the same set of samples: pristine SMA wire, and SMA wires laser-anchored at 15 watts and 17.5 watts. The voltage levels applied were again 5 V, 5.5 V, 6 V, and 6.5 V. Interestingly, across all voltage levels, the laser-anchored wires consistently demonstrated superior angular velocity compared to the pristine wire. This improvement in angular velocity can be attributed to the lower angular displacement observed in laser-anchored wires, which resulted in shorter actuation times. As a result, despite their reduced angular displacement, the quick response time of the laser-anchored wires translated to higher angular velocities. This finding underscores the enhanced dynamic performance of laser-anchored SMA wires, making them advantageous for applications where rapid actuation and high-speed responses are critical.

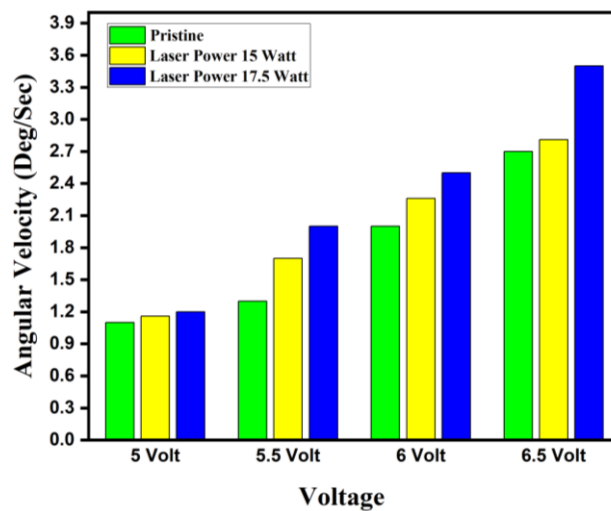


*Figure 19: Angular Velocity Vs Voltage*

### 5.4. Number of Cycles per Minute and Voltage

To further evaluate the dynamic performance of the fabricated actuators, we ran the samples for a duration of one minute and recorded the number of actuation cycles completed within this period. The same set of samples—pristine SMA wire and SMA wires laser-anchored at 15 watts and 17.5 watts—were subjected to this test. The results indicated that the laser-anchored samples completed a greater number of cycles per minute compared to the pristine wire in almost all cases.

This increased cycle frequency in the laser-anchored wires can be attributed to their higher angular



velocity, as previously discussed. The reduced actuation time allowed the laser-anchored wires to complete more cycles within the same timeframe. This enhanced cyclic performance highlights the effectiveness of laser anchoring in improving the responsiveness and operational speed of SMA actuators. Consequently, laser-anchored SMA wires demonstrate a significant advantage in applications requiring high-frequency actuation, offering reliable and rapid performance over extended periods.

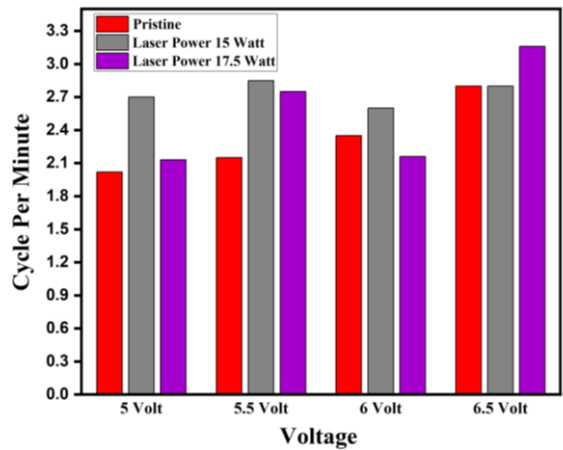


*Figure 20: No. of Cycles per Minute Vs Voltage*

### 5.5. Angular Displacement at Different Frequencies and Voltage

To comprehensively assess the performance of the actuators, we ran the samples at different frequencies: 0.1 Hz, 0.125 Hz, 0.167 Hz, 0.25 Hz, and 0.5 Hz. Correspondingly, the samples were operated for 10 seconds, 8 seconds, 6 seconds, 4 seconds, and 2 seconds, respectively. This range of frequencies allowed us to observe the actuators' behavior under various dynamic conditions.

In nearly all cases, the laser-anchored samples outperformed the pristine SMA wire. The laser-anchored wires consistently demonstrated better results in terms of actuation cycles completed within the specified durations. This superior performance can be attributed to the increased angular velocity and enhanced adhesion between the SMA and PDMS, which reduced slippage and improved efficiency. These findings underscore the advantages of laser anchoring in enhancing the responsiveness and reliability of SMA actuators, making them well-suited for high-frequency

applications where rapid and consistent actuation is essential.

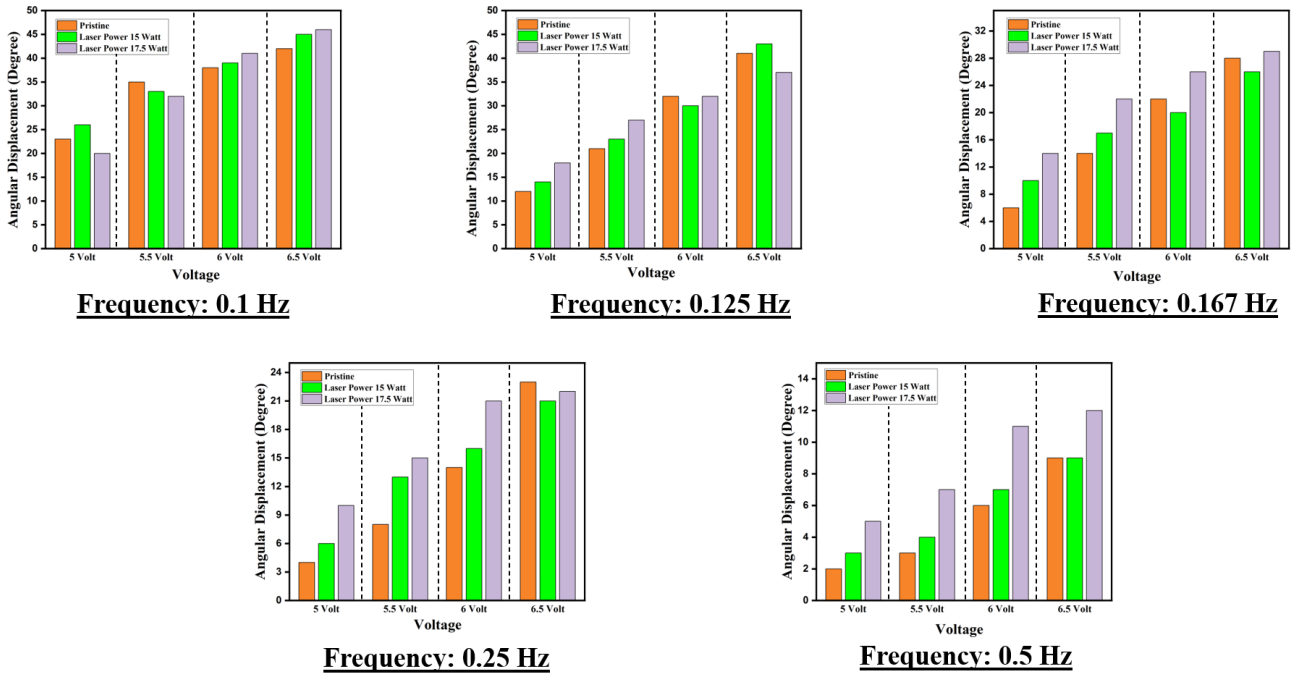


**Figure 21: Angular Displacement vs. voltage at different Frequencies**

## 5.6. Conclusion

The phase transformation analysis revealed that laser-anchored SMA wires exhibit significantly lower transformation temperatures compared to pristine wires. Specifically, the Austenite Start, Austenite Finish, Martensite Start, and Martensite Finish temperatures for the laser-anchored wire were considerably lower. This reduction in phase transformation temperatures translates to decreased power requirements for achieving actuation. Consequently, at the same power levels, laser-anchored SMA wires provide enhanced actuation performance, demonstrating greater efficiency and responsiveness.

Overall, the results from the various tests, including angular displacement, angular velocity, and cycle frequency, indicate that laser-anchored SMA wires generally outperform pristine wires, especially at higher voltage levels and frequencies. The increased angular velocity and higher number of cycles per minute for laser-anchored wires underscore their superior dynamic performance. Additionally, the enhanced adhesion and reduced slippage achieved through laser anchoring contribute to their improved operational reliability and precision. These findings underscore the potential of laser-anchored SMA wires in advanced actuation applications, particularly in underwater soft robotics, where high efficiency, rapid response, and reliable performance are crucial.

## **References**

- [1] Soft robotics: Technologies and systems pushing the boundaries of robot abilities Cecilia Laschi,<sup>1</sup> \* Barbara Mazzolai,<sup>2</sup> Matteo Cianchetti<sup>1</sup>
- [2] Soft Robotics George M. Whitesides\*
- [3] Soft Robotics: A Review of Recent Developments of Pneumatic Soft Actuators James Walker <sup>1</sup> , Thomas Zidek <sup>1</sup> , Cory Harbel <sup>1</sup> , Sanghyun Yoon <sup>1</sup> , F. Sterling Strickland <sup>2</sup> , Srinivas Kumar <sup>1</sup> and Minchul Shin <sup>1</sup>,\*
- [4] Cecilia Laschi • Jonathan Rossiter Fumiya Iida • Matteo Cianchetti Laura Margheri Editors Soft Robotics: Trends, Applications and Challenges Proceedings of the Soft Robotics Week, April 25–30, 2016, Livorno, Italy
- [5] Soft Robot Review Chiwon Lee, Myungjoon Kim, Yoon Jae Kim, Nhayoung Hong, Seungwan Ryu, H. Jin Kim, and Sungwan Kim\*
- [6] Soft Actuators for Soft Robotic Applications: A Review Nazek El-Atab, Rishabh B. Mishra, Fhad Al-Modaf, Lana Joharji, Aljohara A. Alsharif, Haneen Alamoudi, Marlon Diaz, Nadeem Qaiser, and Muhammad Mustafa Hussain
- [7] W. Wang, J. Lee, H. Rodrigue, S. Song, W. Chu, and S. Ahn, “Locomotion of inchworm-inspired robot made of smart soft composite ( SSC ),” vol. 046006.
- [8] S. Seok, C. D. Onal, K. Cho, R. J. Wood, D. Rus, and S. Kim, “Meshworm : A Peristaltic Soft Robot With Antagonistic Nickel Titanium Coil Actuators,” vol. 18, no. 5, pp. 1485–1497, 2013.
- [9] A. Villanueva, C. Smith, and S. Priya, “A biomimetic robotic jellyfish (Robojelly) actuated by shape memory alloy composite actuators,” *Bioinspiration and Biomimetics*, 2011.
- [10] Y. Ko, S. Na, Y. Lee, and K. Cha, “A jellyfish-like swimming mini-robot actuated by an electromagnetic actuation system,” vol. 057001, 2012.
- [11] S. Yeom, J. Jeon, H. Kim, B. Youn, and I. Oh, “Bio-inspired Jellyfish Robots based on Ionic-type Artificial Muscles,” pp. 69–72.
- [12] J. Xiao, J. Duan, and J. Yu, “Design and Implementation of A Novel Biomimetic Robotic Jellyfish,” 2013 IEEE Int. Conf. Robot. Biomimetics, no. December, pp. 988– 993, 2013.
- [13] J. Frame, N. Lopez, O. Curet, and E. D. Engeberg, “Thrust force characterization of free-swimming soft robotic jellyfish,” 2018.
- [14] K. J. Cho, E. Hawkes, C. Quinn, and R. J. Wood, “Design, fabrication and analysis of a body-caudal fin propulsion system for a microrobotic fish,” in *Proceedings -IEEE International Conference on Robotics and Automation*, 2008.
- [15] Z. Wang, Y. Wang, J. Li, and G. Hang, “A micro biomimetic manta ray robot fisactuated by SMA,”

in 20 A. Ravalli, C. Rossi, and G. Marrazza, “Bio-inspired fish robot based on chemicalsensors,” *Sensors Actuators, B Chem.*, 2017.

[16 ]09 IEEE International Conference on Robotics and Biomimetics, ROBIO 2009, 2009.